

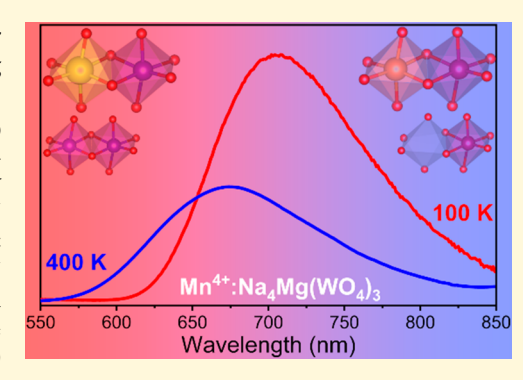
Bandshift Luminescence Thermometry Using Mn⁴⁺:Na₄Mg(WO₄)₃ **Phosphors**

Dinesh K. Amarasinghe and Federico A. Rabuffetti*

Department of Chemistry, Wayne State University, Detroit, Michigan 48202, United States

Supporting Information

ABSTRACT: The feasibility of employing Mn4+-activated phosphors for bandshift luminesence thermometry is demonstrated for the first time using Mn^{4+} : $Na_4Mg(WO_4)_3$. Substitution of Mn^{4+} for Mg^{2+} in $Na_4Mg(WO_4)_3$ yields phosphors in which Mn⁴⁺ activators are distributed over (Na/Mg)₂O₁₀ dimers. Neutron powder diffraction reveals that metal-oxygen bond distances in these dimers are significantly longer than those typically observed in Mn4+-activated phosphors. Multisite distribution of Mn4+ activators coupled to long metal-oxygen distances impart thermometric functionality to Mn⁴⁺:Na₄Mg(WO₄)₃. Red emission from two distinct Mn⁴⁺ emitters leads to a broad band extending from 560 to 850 nm. Differential thermal quenching of these emitters drives a sigmoidal blueshift of the emission maximum upon increasing temperature from 100 to 400 K (ca. 30 nm); bandshift luminescence thermometry is thus realized. Quantitative



assessment of the thermometric performance of Na₄Mg_{0.940}Mn_{0.030}(WO₄)₃ yields a sensitivity of 0.127 nm K⁻¹, a repeatability greater than 99%, and a temperature resolution of 2.5 K at 300 K. Findings presented in this article expand the scope of applicability of Mn⁴⁺-activated thermosensitive phosphors beyond ratiometric bandshape and lifetime thermometry. More importantly from the perspective of developing new phosphors, our results provide structural guidelines for discovering and screening novel oxide hosts for Mn⁴⁺ activators.

■ INTRODUCTION

Luminescent thermometers offer several advantages over routinely used contact and noncontact thermal probes such as thermocouples and pyrometers. Among these advantages are the ability to probe temperature with submicrometric spatial resolution and to function in scenarios where contact thermometry and pyrometry are problematic to implement. The use of thermosensitive phosphors as temperature sensors is tied to the ability to design materials with targeted sensitivity and resolution over the temperature range of interest. From this perspective, a continuous search exists for design principles and materials that go beyond rare-earth-based luminescent thermometers.

Mn⁴⁺-activated phosphors have been extensively studied as red emitters for phosphor-converted white LEDs because they exhibit narrow and tunable emission arising from the ${}^{2}E \rightarrow {}^{4}A_{2}$ transition. Despite thermal quenching being a well-known feature of these materials, much less attention has been paid to their use as thermosensitive phosphors for luminescence thermometry; only a dozen studies have been recently published. 1-12 In these investigations, Mn⁴⁺ activators were doped into oxide or oxyfluoride hosts and thermometric scales were established using temperature-dependent luminescence intensity ratios (ratiometric bandshape thermometry)^{2,3,5-7,9,12} or excited-state lifetimes of Mn⁴⁺ (lifetime thermometry). 1,4,7,8,10,11 To the best of our knowledge, the position of the red emission maximum has not been used as a

thermometric parameter (bandshift thermometry). Bandshift luminescent thermometers are largely dominated by quantum dots and semiconducting nanocrystals. 13-18 These nanomaterials, however, operate in a narrow temperature window (ca. -20 to 120 °C), and repeatability critically depends on colloidal synthetic routes that are not as robust as solid-state reactions employed to synthesize inorganic phosphors. Developing Mn⁴⁺-activated phosphors capable of serving as bandshift thermometers creates the opportunity to address both deficiencies and expands the scope of applicability of these phosphors in luminescence thermometry.

In this work, we use Mn⁴⁺:Na₄Mg(WO₄)₃ to realize bandshift luminescence thermometry between 100 and 400 K. Over the past few years, our group has been investigating oxides featuring group V and group VI d⁰ oxoanions as host materials for thermosensitive phosphors. In particular, we have been looking at hosts in which activator ions may be doped into multiple sites. Multisite distribution of activators may be exploited for luminescence thermometry under the hypothesis that different local atomic environments lead to distinct thermal quenching of each emitting center. In the course of our studies, we discovered the potential of Na₄Mg(WO₄)₃ as a host material for Mn⁴⁺. Na₄Mg(WO₄)₃ was first synthesized by

Received: September 21, 2019 Revised: November 7, 2019 Published: December 3, 2019

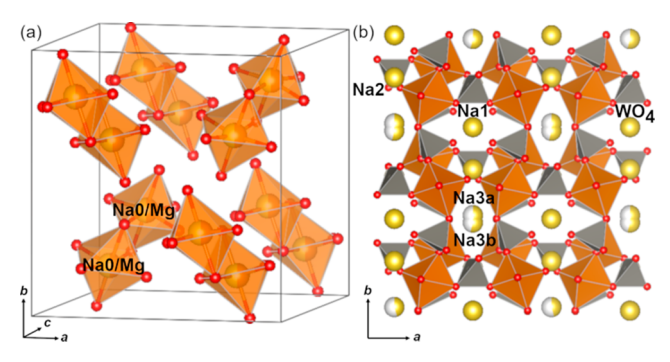


Figure 1. Crystal structure of $Na_4Mg(WO_4)_3$. (a) $(Na/Mg)_2O_{10}$ dimers formed by edge-sharing $(Na/Mg)O_6$ octahedra; sodium and tungsten atoms are not shown. (b) Structure projection onto the (001) plane.

Han et al., and its crystal structure is shown in Figure 1. 19 It crystallizes in the monoclinic C2/c space-group (No. 15), and the most relevant structural feature is the presence of (Na/ Mg)₂O₁₀ dimers formed by edge-sharing (Na/Mg)O₆ octahedra (Figure 1a). Metal sites in these dimers, labeled Na0/Mg hereafter, show occupational disorder of Na+ and Mg²⁺ cations. (Na/Mg)₂O₁₀ dimers are connected to each other by WO₄ tetrahedra to form a three-dimensional framework. When visualized along the c axis, this framework gives rise to channels in which the remaining Na+ cations are located (Figure 1b). Three distinct Na+ cations are present in these channels; these are labeled Na1, Na2, Na3a, and Na3b. The latter two are positionally disordered over the same site. In the following, we demonstrate that doping Mn⁴⁺ into (Na/ Mg)₂O₁₀ dimers yields a bandshift luminescent thermometer operating between 100 and 400 K. Emphasis is placed on elucidating the structural basis of the observed temperaturedependent luminescence response of Mn⁴⁺:Na₄Mg(WO₄)₃. Structure-luminescence relationships are highlighted from the perspective of designing Mn⁴⁺-activated thermosensitive phosphors via rational selection of the host oxide.

■ EXPERIMENTAL SECTION

Synthesis of $Na_4Mg_{1-2x}Mn_x(WO_4)_3$. Solid-state reactions were employed to synthesize polycrystalline $Na_4Mg_{1-2x}Mn_x(WO_4)_3$ (x = 0.000, 0.005, 0.010, 0.020, 0.030, 0.040, 0.050, 0.060, and 0.070). Stoichiometric amounts of Na₂CO₃ (99.5%, Sigma-Aldrich), MgO (99.99%, Alfa Aesar), MnO₂ (99.99%, Sigma-Aldrich), and WO₃ (99.9%, Sigma-Aldrich) were mixed and ground in an agate mortar. The unreacted mixtures were first placed in alumina crucibles and heated under air at 450 °C for 2 h to decompose Na₂CO₃. Then, they were heated at 675 °C for 12 h. After intermediate grinding, polycrystalline samples were reheated three times at 675 °C under identical conditions. Heating rates of 1 °C min⁻¹ were employed throughout. Off-white to pale pink powders were obtained. The oxidation state of manganese was confirmed using X-ray photoelectron spectroscopy (Figure S1). Attempts to synthesize $Na_4Mg_{1-2x}Mn_x(WO_4)_3$ phosphors in which x > 0.070 or phosphors in which Mn^{4+} substitutes for Na^+ (i.e., $Na_{4(1-4x)}MgMn_{4x}(\bar{WO}_4)_3$) led to secondary phases.

Inductively Coupled Plasma Mass Spectrometry (ICP–MS). Elemental analyses of Mn and Mg in $Na_4Mg_{1-2x}Mn_x(WO_4)_3$ were carried out using a 7700 Series ICP–MS (Agilent Technologies). Approximately 2–3 mg of powder was dissolved in 20 mL of aqua regia at room temperature. Manganese and magnesium in 2% HNO₃ (1000 μ g mL⁻¹, High Purity Standards) were used as standards.

Thermal Analysis. Thermogravimetric and differential thermal analyses were conducted using an SDT2960 TGA-DTA analyzer (TA Instruments). Approximately 5–10 mg of powder was first

heated at 35 $^{\circ}C$ for 30 min under flowing nitrogen (100 mL min $^{-1}$). Then, the temperature was ramped to 850 $^{\circ}C$ at a rate of 10 $^{\circ}C$ min $^{-1}$.

Time-of-Flight Neutron Powder Diffraction (TOF–NPD). TOF–NPD data of $Na_4Mg_{1-2x}Mn_x(WO_4)_3$ (x=0.000, 0.010, 0.030, 0.050, 0.070) were collected on the POWGEN beamline of the Spallation Neutron Source (SNS) at Oak Ridge National Laboratory. Approximately 2–3 g of powder were loaded into a 6 mm diameter vanadium can, and diffraction patterns were collected at 300 (all samples) and 100 K (x=0.030). Patterns were recorded with the high-resolution setting and a center wavelength of 0.800 Å in the 4.5–210 ms time window.

Rietveld Analysis. Rietveld refinements of NPD patterns were performed using the General Structure Analysis System (GSAS) with the graphical user interphase (EXPGUI).^{20,21} Crystal structures were refined using the monoclinic space group C2/c (No. 15). The following parameters were refined: (1) scale factor; (2) background, which was modeled using a reciprocal interpolation function; (3) peak shape, which was modeled using TOF peak profile function number 3; (4) diffractometer constant; (5) lattice constants; (6) fractional atomic coordinates when allowed by symmetry; (7) anisotropic displacement parameters except for Na3a and Na3b, for which isotropic displacement parameters (U^{iso}) were refined; and (8) occupancies of the Na3a (f_{Na3a}) and Na3b (f_{Na3b}) sites constrained to $f_{\text{Na3a}} + f_{\text{Na3b}} = 1.00$. The occupancy of the Na0/Mg/Mn site was fixed according to a Na:Mg:Mn molar ratio of 0.500:Mg:Mn; Mg:Mn ratios were obtained from elemental analysis. Difference curves and $R_{\rm wp}$ residuals were employed to assess the quality of the refined structural models. Crystal structures were visualized using VESTA.²

Spectrofluorometry. Spectrofluorometric analyses were conducted using a Fluorolog 3-222 fluorometer (Horiba Scientific). Room-temperature steady-state spectra were collected using a 450 W xenon lamp as the excitation source and a photomultiplier tube R928 as the detector. A slit width of 2 nm and appropriate long-pass filters were employed. Room-temperature luminescence decays were recorded using a 265 nm SpectraLED (Horiba Scientific) as the excitation source. Variable-temperature excitation and emission spectra and luminescence decays were collected for Na₄Mg_{0.940}Mn_{0.030}(WO₄)₃, which showed the highest emission intensity at room temperature. $Na_4Mg_{0.940}Mn_{0.030}(WO_4)_3$ was loaded into a VPF-800 variable-temperature stage (Janis Research Company) and degassed at 650 K for 12 h prior to data collection. A 450 W xenon lamp and a xenon flashlamp were used as the excitation sources to record steady-state spectra and luminescence decays, respectively. A Lake Shore 335-3060 controller (Lake Shore Cryotronics, Inc.) provided temperature readings with ± 0.2 K accuracy. A heating rate of 5 K min⁻¹ was employed.

■ RESULTS AND DISCUSSION

We first analyzed the chemical purity of $a_4Mg_{1-2x}Mn_x(WO_4)_3$ phosphors; emphasis was placed on probing the incorporation of Mn⁴⁺ into the host lattice. Results from elemental analyses of Mg and Mn are plotted in Figure 2; numeric results are given in the Supporting Information (Table S1). An excellent agreement is observed between the nominal and experimental Mn⁴⁺ contents (Figure 2a) and Mn:Mg molar ratios (Figure 2b). Both results demonstrate that Mn⁴⁺ substitutes for Mg²⁺ in the Na0/Mg site in $(Na/Mg)_2O_{10}$ dimers and that Mn^{4+} does not replace Na+ to an observable extent. This was expected on the basis of the much larger mismatch between the crystal radii of Na+ and Mn4+ than between those of Mg2+ and Mn⁴⁺ (1.02 Å for Na⁺, 0.72 Å for Mg²⁺, and 0.53 Å for Mn⁴⁺ in octahedral coordination).²³ The strong preference of Mn⁴⁺ to substitute for Mg²⁺ instead of Na⁺ is also in agreement with the observation that attempting to synthesize $Na_{4(1-4x)}MgMn_{4x}(WO_4)_3$ invariably leads to secondary phases (Figure S2). Thermal analyses confirm the chemical purity of

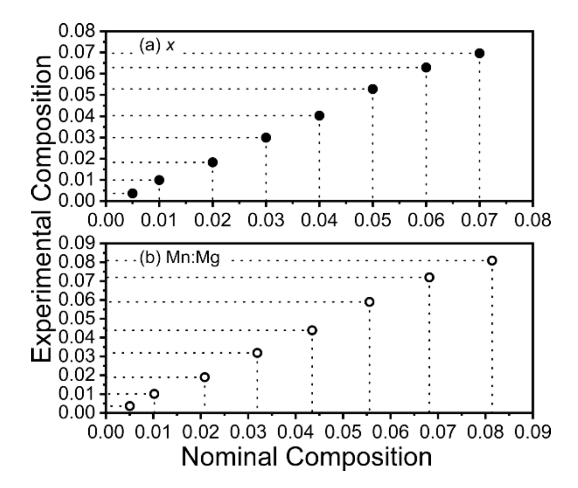


Figure 2. Elemental analysis of $Na_4Mg_{1-2x}Mn_x(WO_4)_3$. Experimental Mn⁴⁺ content (a) and Mn:Mg molar ratio (b) as a function of their nominal values.

 $Na_4Mg_{1-2x}Mn_x(WO_4)_3$ phosphors. No additional exo- or endothermic peaks appear in the DTA curves upon incorporation of Mn4+ and melting points remain nearly constant throughout the series (773 °C for x = 0.000 and 765 °C for x = 0.070; see Figure S3).

Next, we probed the crystal structure of $Na_4Mg_{1-2x}Mn_x(WO_4)_3$. Structural analysis aimed to determine metal—oxygen distances and bond angles for the Na0/Mg/Mn site. These geometric parameters determine the strength and symmetry of the crystal field experienced by the Mn⁴⁺ activator and, as result, directly affect emission from d-d transitions. Rietveld analyses of neutron diffraction patterns of $Na_4Mg_{0.940}Mn_{0.030}(WO_4)_3$ at 100 and 300 K are shown in Figure 3; selected structural parameters at 300 K are listed in Table 1. Results from analyses of other compositions are provided in the Supporting Information (Figure S4 and Tables S2-S9). NPD confirms the phase purity of the sample as all diffraction maxima are indexed to the Na₄Mg(WO₄)₃ phase; no secondary crystalline phases are observed. Inspection of difference curves and $R_{\rm wp}$ residuals demonstrates that the average crystal structure of the phosphor is adequately described by the structural model first proposed by Han et al. 19 This model holds equally well at low and room temperatures. Large displacement parameters are obtained for the Na3a and Na3b sites at 100 and 300 K, as expected on the basis of their positional disorder along the b axis (see Table S2). Equivalent displacement parameters (U^{eq}) obtained from anisotropic refinement of the occupationally disordered Na0/ Mg/Mn site at 300 K show no significant dependence on the Mn⁴⁺ content (1.64 Å² for x = 0.000 vs 1.53 Å² for x = 0.070). Based on structural parameters extracted from Rietveld analyses, the average atomic environment of Mn⁴⁺ in (Na/ Mg)₂O₁₀ dimers may be depicted as follows. Metal sites in these dimeric units exhibit C_1 symmetry and have six oxide anions in a distorted octahedral geometry as nearest neighbors. Metal-oxygen bond distances range from 2.144 to 2.360 Å and most oxygen-metal-oxygen angles deviate significantly from 90° (see Table S9). The presence of occupationally disordered (Na/Mg)₂O₁₀ dimeric units in the undoped host lattice leads to a statistical distribution of NaMgO₁₀, Mg₂O₁₀, and Na₂O₁₀ dimers. Upon doping, Mn⁴⁺ substitutes for Mg in $NaMgO_{10}$ and Mg_2O_{10} dimers. Four different local environments for Mn^{4+} may therefore be envisioned; these

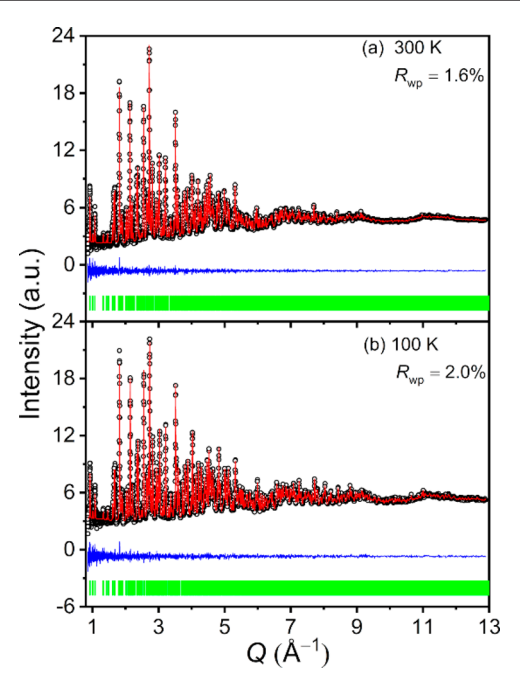


Figure 3. Rietveld analysis of NPD patterns of Na₄Mg_{0.940}Mn_{0.030}(WO₄)₃ at (a) 300 and (b) 100 K. Experimental data (black circles), calculated patterns (red curve), and difference curves (blue, offset for clarity) are shown. Tick marks corresponding to the calculated position of the diffraction maxima are depicted as green vertical bars.

Table 1. Structural Parameters of Na₄Mg_{0.940}Mn_{0.030}(WO₄)₃ at 300 K

```
a (Å)
                                                             12.6058(3)
       b (Å)
                                                            13.6203(3)
       c (Å)
                                                            7.1904(13)
       \beta (deg)
                                                            111.920(11)
       V(Å^3)
                                                            1145.31(5)
                                                            0.2900(3), 0.3415(2), 0.3786(4)
       (x, y, z)_{\text{Na0/Mg/Mn}}
                                                             -0.0216(17), 0.0287(18)
       y<sub>Na3a</sub>, y<sub>Na3b</sub>
      f_{\rm Na3a}, f_{\rm Na3b}
                                                            0.53(2), 0.47(2)
       U^{eq}_{\rm Na0/Mg/Mn}~({\rm \AA}^2)^{a,b}
                                                            1.52(8)
       U^{iso}_{\text{Na3a}} = U^{iso}_{\text{Na3b}} (\text{Å}^2)^a
                                                            3.9(2)
       \langle Na0/Mg/Mn-O \rangle (Å)
                                                            2.215
       R<sub>wp</sub> (%)
<sup>a</sup>Given as 100 × U. <sup>b</sup>U<sup>eq</sup> = \frac{1}{3} × (U<sup>11</sup> + U<sup>22</sup> + U<sup>33</sup>).
```

are (1) NaMnO₁₀ dimers resulting from Mn⁴⁺ replacing Mg²⁺

in NaMgO₁₀ dimers (Figure 4a); (2) MgMnO₁₀ and Mn₂O₁₀ dimers arising from substitution in Mg₂O₁₀ dimers (Figures 4b,c); and (3) Mn \square O₁₀ dimers created when Mn⁴⁺ ions occupy a Mg^{2+} site adjacent to a Mg^{2+} vacancy (\square) generated to maintain charge balance (Figure 4d). Owing to the low doping level of the phosphors, we expect Mn⁴⁺ activators to be primarily located in NaMnO₁₀ and MgMnO₁₀ dimers rather than in Mn₂O₁₀ and Mn \square O₁₀. Mn₂O₁₀ dimeric units may occur at higher doping levels or in the case of prominent clustering effects; first-principles calculations by Wang et al. have indeed shown the high formation of energy of Mn⁴⁺-Mn⁴⁺ pairs.²⁴ Besides a multisite distribution of Mn⁴⁺ activators, a unique structural feature of Na₄Mg_{1-2x}Mn_x(WO₄)₃ is the length of metal-oxygen bonds extracted for the Na0/Mg/Mn site. These distances are significantly longer than those reported in previous inves-

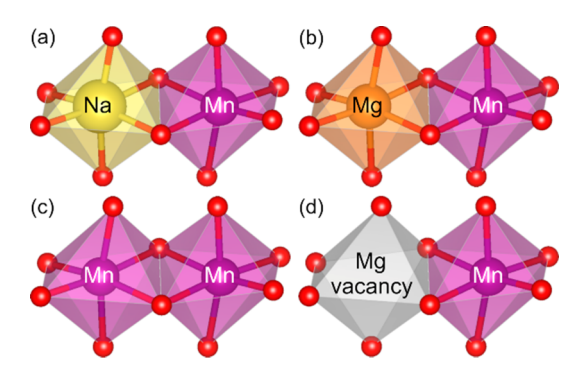


Figure 4. Four different local environments for Mn^{4+} may result upon substitution for Mg^{2+} in $(Na/Mg)_2O_{10}$ dimers.

tigations of $\mathrm{Mn^{4+}}$ -activated phosphors: they range from 2.14 to 2.36 Å whereas previously studied phosphors feature distances ranging from 1.80 to 2.05 Å (see Table S10). On this basis, one may expect $\mathrm{Mn^{4+}}$ to experience a weaker crystal field when doped into $\mathrm{Na_4Mg(WO_4)_3}$. In the following paragraphs we demonstrate that multisite distribution of $\mathrm{Mn^{4+}}$ activators experiencing a weak crystal field not only servess to rationalize the luminescence response of $\mathrm{Na_4Mg_{1-2x}Mn_x(WO_4)_3}$ phosphors but also imparts thermometric functionality.

Luminescence was first probed as a function of the Mn⁴⁺ content. Room-temperature excitation spectra were collected between 230 and 640 nm ($\lambda_{\rm em} = 682$ nm), and emission spectra were collected between 400 and 850 nm ($\lambda_{\rm exc}$ = 253 nm); these are shown in Figure 5a. Excitation spectra are dominated by an asymmetric oxygen-to-metal charge-transfer band (CTB) centered at ≈253 nm. Much weaker bands arising from Mn^{4+} d-d transitions are observed in the 350-600 nm range (Figure S5). Radiative relaxation of Mn4+ leads to an asymmetric broad red band centered at ≈682 nm, which we tentatively assign to the ${}^4T_2 \rightarrow {}^4A_2$ transition of the Mn⁴⁺ activator in octahedral coordination. This result is in contrast with previous investigations of Mn⁴⁺-containing phosphors that typically observe narrow red emission resulting from the ${}^{2}E \rightarrow$ 4A_2 transition and the corresponding vibronic transitions. ²⁵ Our tentative assignment of broadband red emission to the 4T_2 \rightarrow ⁴A₂ transition instead of broadened vibronic emission from the ²E state is based on spectroscopic and structural data. Indeed, no narrow bands or fine spectral features are observed

in the emission spectra of Na₄Mg_{1-2x}Mn_x(WO₄)₃ phosphors even at 78 K. In addition, metal-oxygen bond distances for the Na0/Mg/Mn site are significantly longer than those reported for the few Mn⁴⁺-activated phosphors for which asymmetric and broadened vibronic emission from the ²E state is observed (type B phosphors in the classification proposed by Adachi²⁵); these are Li₂Mg₂Ti₃O₈ (1.90-2.02 Å)²⁶ and Li₂MgTiO₄ (2.08 Å).²⁷ Longer metal-oxygen distances lead to a weaker crystal field and, 28 ultimately, to broadband red emission from $\mathrm{Mn}^{4+29-32}$ Emission intensities increase up to x=0.030 and then decrease due to concentration quenching (see inset of Figure 5a). The position and shape of the red emission band, on the other hand, does not change with the Mn⁴⁺ content. As shown in Figure 5b for the case of Na₄Mg_{0.940}Mn_{0.030}(WO₄)₃, this band exhibits a pronounced asymmetry. We attribute this feature to Mn4+ emitters distributed over more than one crystallographic site. The presence of four different dimeric units in which Mn⁴⁺ ions may sit provides the structural basis for this observation. As mentioned earlier, we expect Mn⁴⁺ activators to be primarily encountered as NaMnO₁₀ and MgMnO₁₀ dimers.

The presence of two distinct Mn⁴⁺ emitters was supported by kinetic analyses of room-temperature decays. Luminescence decays were monitored at 682 nm under 265 nm excitation. Results from these analyses are summarized in Figure 6; here the lifetimes of the long- and short-lived Mn⁴⁺ emitters and their fractional contribution to the total emission intensity are plotted as a function of the Mn⁴⁺ content. Experimental decay curves and numeric results used in these plots are given in the Supporting Information (Figure S6 and Table S11). All decays were adequately fit with a biexponential function given by eq 1, where I(t) is the luminescence intensity at time t, τ_{LL} and τ_{SL} are the excited-state lifetimes of the long- (LL) and short-lived (SL) Mn^{4+} emitters, respectively, and A, A_{LL} , and A_{SL} are constants. The fractional contributions of each emitter (F_{LL} and F_{SL}) to the total emission intensity were computed using egs 2 and 3.

$$I(t) = A + A_{LL} \exp\left(-\frac{t}{\tau_{LL}}\right) + A_{SL} \exp\left(-\frac{t}{\tau_{SL}}\right)$$
(1)

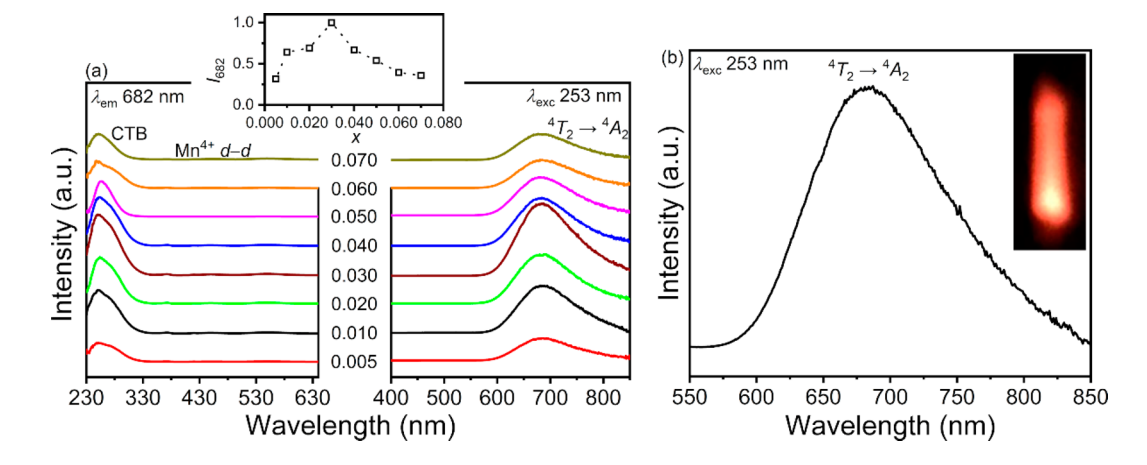


Figure 5. (a) Room-temperature excitation and emission spectra of $Na_4Mg_{1-2x}Mn_x(WO_4)_3$ phosphors. Inset: normalized integrated intensity of the red emission band centered at 682 nm as a function of the Mn^{4+} content. (b) Red emission band of $Na_4Mg_{0.940}Mn_{0.030}(WO_4)_3$. Inset: red emission under 253 nm illumination.

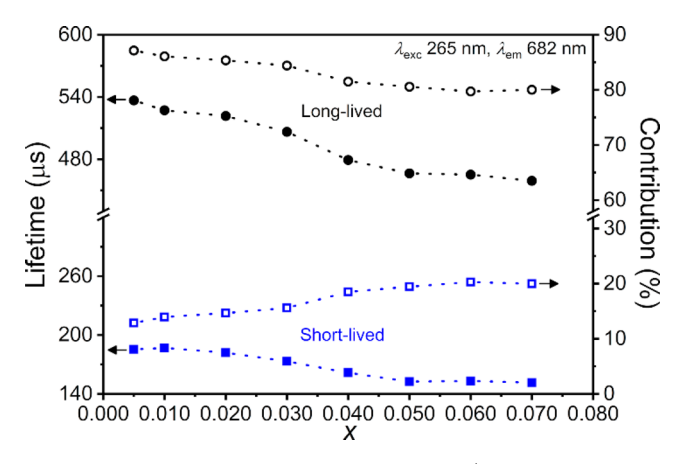


Figure 6. Lifetimes of long- and short-lived Mn⁴⁺ emitters and their fractional contributions to red emission as a function of the Mn⁴⁺ content. Decays were collected at room temperature. Dotted lines are guides to the eye.

$$F_{LL} = \frac{\tau_{LL} A_{LL}}{\tau_{LL} A_{LL} + \tau_{SL} A_{SL}} \tag{2}$$

$$F_{SL} = \frac{\tau_{SL} A_{SL}}{\tau_{LL} A_{LL} + \tau_{SL} A_{SL}} \tag{3}$$

The observation of biexponential decays confirms the presence to two distinct Mn^{4+} emitters. Red emission is dominated by a long-lived emitter with lifetimes ranging from ≈ 540 to $450~\mu\mathrm{s}$. A minor contribution from a short-lived emitter with lifetimes ranging from ≈ 185 to $150~\mu\mathrm{s}$ is also observable. The contribution of the short-lived emitter increases from 13 to 20% upon increasing the concentration of Mn^{4+} , indicating the preferential incorporation of Mn^{4+} in one dimeric unit.

The temperature dependence of the luminescence of $Na_4Mg_{1-2x}Mn_x(WO_4)_3$ phosphors was probed to screen their potential as optical thermometers. Emphasis was placed on establishing whether the thermal quenching characteristics of the two Mn4+ emitters were different enough to yield an observable change in spectral distribution upon changing temperature. Variable-temperature luminescence measurements were conducted on Na₄Mg_{0.940}Mn_{0.030}(WO₄)₃. Results from these studies are summarized in Figure 7. Inspection of the emission spectrum in Figure 7a shows that, as expected, the intensity of the red emission band decreases with temperature. More importantly, its maximum shows a large blueshift from \approx 709 to 675 nm upon increasing temperature from 78 to 400 K. Analysis of temperature-dependent luminescence decays reveals that this blueshift stems from the distinct thermal quenching characteristics of the two Mn⁴⁺ emitters contributing to red emission. Biexponential decays were monitored at 682 nm and fit to extract the temperature-dependent lifetimes of the long- $(\tau_{IJ}(T))$ and short-lived emitters $(\tau_{SI}(T))$. Next, the corresponding effective rate constants ($k_{LL}^{eff}(T)$ and $k_{SL}^{eff}(T)$) were fit using a single-barrier model given by eqs 4 and 5.

$$k_{LL}^{eff}(T) = \frac{1}{\tau_{LL}(T)} = k_{LL}^{R} + k_{LL}^{NR0} \exp\left(-\frac{E_a^{LL}}{k_B T}\right)$$
 (4)

$$k_{SL}^{eff}(T) = \frac{1}{\tau_{SL}(T)} = k_{SL}^{R} + k_{SL}^{NR0} \exp\left(-\frac{E_a^{SL}}{k_B T}\right)$$
(5)

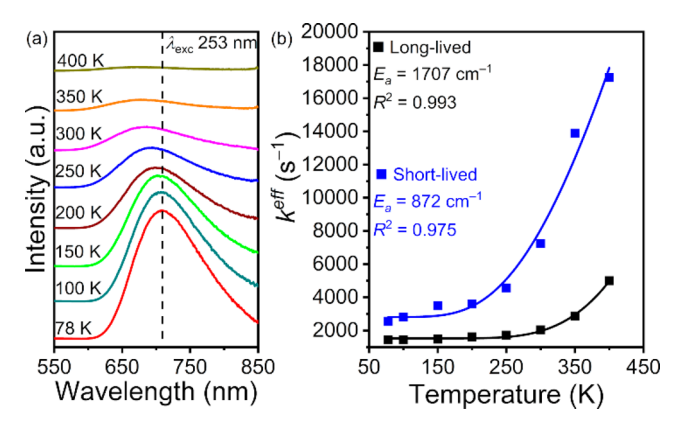


Figure 7. (a) Temperature-dependent emission spectrum of $Na_4Mg_{0.940}Mn_{0.030}(WO_4)_3$. The maximum of the red emission band centered at 682 nm blueshifts upon increasing temperature. (b) Fits of the single-barrier model to the effective rate constant of the 4T_2 state of the long- and short-lived Mn^{4+} emitters. Fits are depicted as solid lines; activation energies (E_a) and fit residuals (R^2) are given.

Here k^R is the radiative constant of the 4T_2 excited state, and k^{NR0} and E_a are the attempt rate and activation energy for nonradiative deactivation via crossover to the ⁴A₂ ground state, respectively. Fits of $k_{LL}^{eff}(T)$ and $k_{SL}^{eff}(T)$ are shown in Figure 7b; experimental decays and corresponding numeric results are given in the Supporting Information (Figure S7 and Tables S12 and S13). The single-barrier model provides an adequate description of the temperature-dependent responses of the two Mn⁴⁺ emitters. Comparison of the activation energies for nonradiative relaxation shows that the short-lived emitter is more prone to thermal quenching than the long-lived emitter (872 vs 1707 cm⁻¹). The observed blueshift of the emission maximum can therefore be rationalized by considering that the long-lived Mn⁴⁺ emits at shorter wavelengths and the shortlived Mn⁴⁺ emits at longer wavelengths. The more pronounced deactivation of the short-lived emitter upon increasing temperature drives the maximum of the red emission band to shorter wavelengths. We note here the relevance of the activation energy required to reach the crossover of the 4T_2 and 4A_2 parabolas for luminescence thermometry, as it enables differential thermal quenching of Mn⁴⁺ emitters.^{8,33,34} Also noteworthy is the fact that, strictly speaking, Na₄Mg_{0.940}Mn_{0.030}(WO₄)₃ is a bandshape thermometer because it is the change in the relative emission intensities of the two Mn⁴⁺ emitters that drives the observed blueshift of the red emission maximum. Throughout this article, however, we use the term "bandshift" because the thermometric parameter utilized to convert optical readings to temperature values is the position of the emission maximum, as described below.

Finally, we exploited the blueshift of the red emission maximum to realize bandshift luminescence thermometry. Studies were conducted to probe the thermometric sensitivity, repeatability, and temperature resolution of Na₄Mg_{0.940}Mn_{0.030}(WO₄)₃. Results are summarized in Figure 8 and figures-of-merit are given in Table 2; spectra and additional numeric data are given in the Supporting Information (Figure S8 and Table S14). We used the centroid of the red emission band ($\lambda_{centroid}$) as the thermometric parameter instead of the intensity maximum. $\lambda_{centroid}$ was computed using eq 6, where $I(\lambda)$ is the emission intensity.

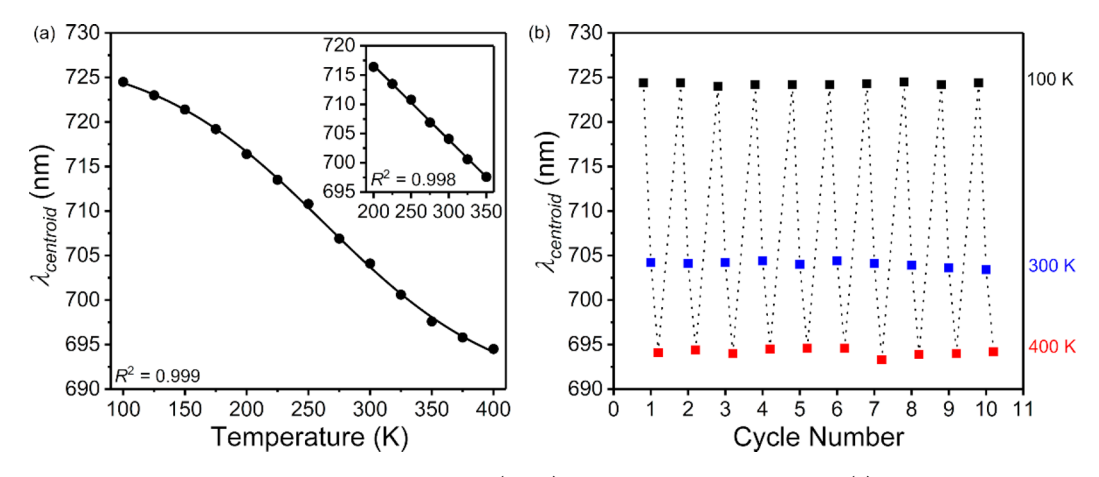


Figure 8. Centroid of the red emission band of $Na_4Mg_{0.940}Mn_{0.030}(WO_4)_3$ as a function of temperature (a) and heating—cooling cycle (b). Solid lines in (a) depict sigmoidal and linear fits in the 100–400 and 200–350 K (inset) temperature ranges, respectively; fit residuals (R^2) are given.

Table 2. Thermometric Performance of $Na_4Mg_{0.940}Mn_{0.030}(WO_4)_3$

temperature (K)	sensitivity (nm K^{-1})	repeatability (%)	$\langle T_{calculated} \rangle^a \ (K)$	resolution (K)
100	0.045	>99	102.0	3.2
300	0.127	>99	297.5	2.5
400	0.061	>99	400.5	6.8

^aArithmetic mean of 10 values.

$$\lambda_{centroid} = \frac{\int \lambda I(\lambda) \, d\lambda}{\int I(\lambda) \, d\lambda} \tag{6}$$

As shown in Figure 8a, $\lambda_{centroid}$ exhibits a sigmoidal dependence on temperature between 100 and 400 K. A Boltzmann function given by eq 7 provides an excellent fit to this dependence; the corresponding fitting parameters are $A_1 = 689.2(9)$ nm, $A_2 = 727.9(7)$ nm, $T_0 = 263(3)$ K, and $\sigma = 72(4)$ K.

$$\lambda_{centroid}(T) = A_2 + \frac{A_1 - A_2}{1 + \exp\frac{T - T_0}{\sigma}}$$
(7)

This function illustrates the transition between an initial regime in which both long- and short-lived Mn⁴⁺ emitters are active and a final regime in which emission is dominated by the long-lived emitter. The thermometric sensitivity of Na₄Mg_{0.940}Mn_{0.030}(WO₄)₃ was estimated by taking the derivative of $\lambda_{centroid}(T)$ with respect to temperature; values of 0.045, 0.127, and 0.061 nm K^{-1} were thus obtained at 100, 300, and 400 K, respectively. We note here that a roomtemperature sensitivity of 0.127 nm K⁻¹ is also obtained if the temperature dependence of $\lambda_{centroid}$ between 200 and 350 K is fit with a linear function of the type $\lambda_{centroid}(T) = -AT + B$, where A = 0.127(2) nm K⁻¹ and B = 742.1(6) nm (see inset of Figure 8a). The room-temperature sensitivity of our Mn⁴⁺activated phosphor is comparable to that reported for bandshift thermometers operating on the basis of bandgap emission from quantum dots and semiconducting nanocrystals, which exhibit sensitivities in the 0.100-0.200 nm K⁻¹ range. 13-17 However, a major advantage of Na₄Mg_{0.940}Mn_{0.030}(WO₄)₃ is its ability to operate over a much broader temperature window; quantum dots and semiconducting nanocrystals are limited to low temperatures (ca. -20 to 120 °C) unless embedded in a solid matrix. 16 This advantage also holds when compared to highly sensitive Ag/

 Ag_2S nanocrystals (≈ 2 nm K⁻¹) that operate between 15 and 50 °C.³⁵ Comparison of the thermometric sensitivity of Na₄Mg_{0.940}Mn_{0.030}(WO₄)₃ with other phosphors used in bandand lineshift thermometry is restricted by the limited number of examples reported in the literature. Notably, Mn⁴⁺-activated phosphors have not been investigated at all as bandshift thermometers; their use has been limited to ratiometric bandshape and lifetime optical thermometry. Among the very few lineshift thermometers based on activator emission that have been reported are $Eu^{3+}:Y_2O_2S$, 36 $Nd^{3+}:LaF_3$, 18 $Ce^{3+}:Y_3Al_5O_{12}$, 37 and $Eu^{3+}/Dy^{3+}:YVO_4$. 38 As expected, sensitively tivity values for Na₄Mg_{0.940}Mn_{0.030}(WO₄)₃ are much higher than those reported for thermosensitive phosphors based on *f* f and f-d transitions (e.g., 0.007 nm K⁻¹ for Nd³⁺:LaF₃). The repeatability of the response of Na₄Mg_{0.940}Mn_{0.030}(WO₄)₃ at 100, 300, and 400 K was evaluated by subjecting the phosphor to 10 heating-cooling cycles and extracting $\lambda_{centroid}$ at the temperature of interest. Cyclability plots are shown in Figure 8b. Repeatability values greater than 99% were computed using eq 8, where $\lambda_{centroid}^{i}(T)$ is the value of $\lambda_{centroid}$ in the *i*th cycle and $\langle \lambda_{centroid}(T) \rangle$ is the mean value of $\lambda_{centroid}$ computed over 10

Repeatability (at T)

$$= 100 \times \left[1 - \frac{\max |\lambda_{centroid}^{i}(T) - \langle \lambda_{centroid}(T) \rangle|}{\langle \lambda_{centroid}(T) \rangle} \right]$$
(8)

Overall, the repeatability of the thermometric response is excellent across the entire temperature range; no signs of thermal hysteresis are observed. Finally, temperature resolution (ΔT) was estimated by applying the thermometric scale given in eq 7 to calculate a series of temperature values $(T_{calculated})$ from the spectra used for repeatability measurements. The standard deviation of these values was used as an estimate of the phosphor's temperature resolutions. Temperature resolutions of 3.2, 2.5, and 6.8 K were obtained at 100, 300, and 400 K, respectively.

CONCLUSIONS

The functionality of Mn^{4+} -activated $Na_4Mg(WO_4)_3$ phosphors as bandshift luminescent thermometers was demonstrated. These phosphors operate in the 100-400 K temperature range with a sensitivity comparable to that of quantum dots previously used as bandshift thermometers. Structural analysis

of $Na_4Mg_{1-2x}Mn_x(WO_4)_3$ revealed that their temperature sensing ability stems from (1) the distribution of Mn^{4+} activators over $(Na/Mg)_2O_{10}$ dimers and (2) metal—oxygen bond distances that are longer than those typically encountered in Mn^{4+} -activated phosphors. These features provided the structural basis to rationalize the observed asymmetric broadband red emission as well as its temperature dependence. A significant blueshift of the red emission maximum occurred upon increasing temperature as a result of differential thermal quenching of two distinct Mn^{4+} activators.

The significance of these findings is two-fold. First, they expand the scope of applicability of Mn⁴⁺-activated phosphors in luminescence thermometry. To the best of our knowledge, $Na_4Mg_{1-2x}Mn_x(WO_4)_3$ is the first example of a bandshift thermometer based on emission from Mn⁴⁺ activators; previously reported phosphors were used as ratiometric bandshape and lifetime thermometers instead. More importantly, structure-luminescence relationships established in this work serve to outline two design principles. Candidate host materials for bandshift thermosensitive phosphors activated by Mn⁴⁺ should be sought among oxides featuring (1) occupational disorder of the site in which Mn⁴⁺ is expected to enter and (2) long bond distances between Mn4+ and the surrounding oxide anions (i.e., > 2.10 Å). Hosts featuring group V and group VI d⁰ oxoanions as building blocks appear to be a good starting point for future developments, particularly considering their chemical and thermal stability.

ASSOCIATED CONTENT

S Supporting Information

The Supporting Information is available free of charge at https://pubs.acs.org/doi/10.1021/acs.chemmater.9b03886.

(1) Elemental and thermal analyses, (2) additional TOF–NPD patterns and crystallographic data, (3) luminescence decays, and (4) thermometric performance of $Na_4Mg_{0.940}Mn_{0.030}(WO_4)_3$ (PDF)

AUTHOR INFORMATION

Corresponding Author

*(F.A.R.) E-mail: far@chem.wayne.edu.

ORCID ®

Federico A. Rabuffetti: 0000-0001-8500-3427

Notes

The authors declare no competing financial interest.

■ ACKNOWLEDGMENTS

The authors would like to acknowledge the financial support of the Research Corporation for Science Advancement for a Cottrell Scholar Award and of Wayne State University's Department of Chemistry. They also thank the Lumigen Instrument Center at Wayne State University for the use of the X-ray diffraction core (National Science Foundation MRI-1427926) and of the UPS/XPS (National Science Foundation MRI-1849578). This research used resources at the Spallation Neutron Source, a DOE Office of Science User Facility operated by the Oak Ridge National Laboratory. Prof. Leopoldo Suescun (Facultad de Química, Universidad de la República, Uruguay) is acknowledged for helpful discussions.

■ REFERENCES

(1) Zhydachevskii, Y.; Galanciak, D.; Kobyakov, S.; Berkowski, M.; Kamińska, A.; Suchocki, A.; Zakharko, Y.; Durygin, A. Photo-

luminescence Studies of Mn⁴⁺ ions in YAlO₃ Crystals at Ambient and High Pressure. *J. Phys.: Condens. Matter* **2006**, *18*, 11385–11396.

- (2) Chen, D.; Liu, S.; Zhou, Y.; Wan, Z.; Huang, P.; Ji, Z. Dual-Activator Luminescence of RE/TM:Y₃Al₅O₁₂ (RE = Eu³⁺, Tb³⁺, Dy³⁺; TM = Mn⁴⁺, Cr³⁺) Phosphors for Self-Referencing Optical Thermometry. *J. Mater. Chem. C* **2016**, *4*, 9044–9051.
- (3) Cai, P.; Qin, L.; Chen, C.; Wang, J.; Seo, H. J. Luminescence, Energy-Transfer and Optical Thermometry of a Novel Narrow Red Emitting Phosphor: Cs₂WO₂F₄:Mn⁴⁺. *Dalton Trans.* **2017**, 46, 14331–14340.
- (4) Li, F.; Cai, J.; Chi, F.; Chen, Y.; Duan, C.; Yin, M. Investigation of Luminescence from LuAG:Mn⁴⁺ for Physiological Temperature Sensing. *Opt. Mater.* **2017**, *66*, 447–452.
- (5) Cai, P.; Qin, L.; Chen, C.; Wang, J.; Bi, S.; Kim, S. I.; Huang, Y.; Seo, H. J. Optical Thermometry Based on Vibration Sidebands in Y₂MgTiO₆:Mn⁴⁺ Double Perovskite. *Inorg. Chem.* **2018**, *57*, 3073–3081
- (6) Cai, P.; Wang, X.; Seo, H. J. Excitation Power Dependent Optical Temperature Behaviors in Mn⁴⁺-Doped Oxyfluoride Na₂WO₂F₄. *Phys. Chem. Chem. Phys.* **2018**, 20, 2028–2035.
- (7) Glais, E.; Đorđević, V.; Papan, J.; Viana, B.; Dramićanin, M. D. MgTiO₃:Mn⁴⁺ a Multi-Reading Temperature Nanoprobe. *RSC Adv.* **2018**, 8, 18341–18346.
- (8) Marciniak, L.; Trejgis, K. Luminescence Lifetime Thermometry with Mn³⁺–Mn⁴⁺ Co-doped Nanocrystals. *J. Mater. Chem. C* **2018**, *6*, 7092–7100.
- (9) Sekulić, M.; Đorđević, V.; Ristić, Z.; Medić, M.; Dramićanin, M. D. Highly Sensitive Dual Self-Referencing Temperature Readout from the Mn⁴⁺/Ho³⁺ Binary Luminescence Thermometry Probe. *Adv. Opt. Mater.* **2018**, *6*, 1800552.
- (10) Venturini, F.; Baumgartner, M.; Borisov, S. M. Mn⁴⁺-Doped Magnesium Titanate—A Promising Phosphor for Self-Referenced Optical Temperature Sensing. *Sensors* **2018**, *18*, 668.
- (11) Dramičanin, M. D.; Milićević, B.; Đorđević, V.; Ristić, Z.; Zhou, J.; Milivojević, D.; Papan, J.; Brik, M. G.; Ma, C.-G.; Srivastava, A. M.; Wu, M. Li₂TiO₃:Mn⁴⁺ Deep-Red Phosphor for the Lifetime-Based Luminescence Thermometry. *ChemistrySelect* **2019**, *4*, 7067–7075.
- (12) Wang, P.; Mao, J.; Zhao, L.; Jiang, B.; Xie, C.; Lin, Y.; Chi, F.; Yin, M.; Chen, Y. Double Perovskite A_2LaNbO_6 : Mn^{4+} , Eu^{3+} (A=Ba, Ca) Phosphors: Potential Applications in Optical Temperature Sensing. *Dalton Trans.* **2019**, *48*, 10062–10069.
- (13) Li, S.; Zhang, K.; Yang, J. M.; Lin, L. W.; Yang, H. Single Quantum Dots as Local Temperature Markers. *Nano Lett.* **2007**, *7*, 3102–3105.
- (14) Maestro, L. M.; Rodriguez, E. M.; Rodriguez, F. S.; la Cruz, M. C. I.; Juarranz, A.; Naccache, R.; Vetrone, F.; Jaque, D.; Capobianco, J. A.; Sole, J. G. CdSe Quantum Dots for Two-Photon Fluorescence Thermal Imaging. *Nano Lett.* **2010**, *10*, 5109–5115.
- (15) Dai, Q. Q.; Zhang, Y.; Wang, Y. N.; Hu, M. Z.; Zou, B.; Wang, Y. D.; Yu, W. W. Size-Dependent Temperature Effects on PbSe Nanocrystals. *Langmuir* **2010**, *26*, 11435–11440.
- (16) Pugh-Thomas, D.; Walsh, B. M.; Gupta, M. C. CdSe(ZnS) Nanocomposite Luminescent High Temperature Sensor. *Nanotechnology* **2011**, *22*, 185503.
- (17) Liang, R.; Tian, R.; Shi, W.; Liu, Z.; Yan, D.; Wei, M.; Evans, D. G.; Duan, X. A Temperature Sensor Based on CdTe Quantum Dots—Layered Double Hydroxide Ultrathin Films via Layer-by-Layer Assembly. *Chem. Commun.* **2013**, *49*, 969–971.
- (18) Rocha, U.; Jacinto da Silva, C.; Ferreira Silva, W.; Guedes, I.; Benayas, A.; Martínez Maestro, L.; Acosta Elias, M.; Bovero, E.; van Veggel, F. C. J. M.; García Solé, J. A.; Jaque, D. Subtissue Thermal Sensing Based on Neodymium-Doped LaF₃ Nanoparticles. *ACS Nano* **2013**, *7*, 1188–1199.
- (19) Han, S.; Wang, Y.; Jing, Q.; Wu, H.; Pan, S.; Yang, Z. Effect of the Cation Size on the Framework Structures of Magnesium Tungstate, $A_4Mg(WO_4)_3$ (A = Na, K), $R_2Mg_2(WO_4)_3$ (R = Rb, Cs). Dalton Trans. 2015, 44, 5810–5817.
- (20) Larson, A. C.; Von Dreele, R. B. General Structure Analysis System (GSAS); Los Alamos National Laboratory: 2000.

(21) Toby, B. EXPGUI, A Graphical User Interface for GSAS. J. Appl. Crystallogr. 2001, 34, 210–213.

- (22) Momma, K.; Izumi, F. VESTA 3 for Three-Dimensional Visualization of Crystal, Volumetric and Morphology Data. *J. Appl. Crystallogr.* **2011**, *44*, 1272–1276.
- (23) Shannon, R. D.; Prewitt, C. T. Effective Ionic Radii in Oxides and Fluorides. *Acta Crystallogr., Sect. B: Struct. Crystallogr. Cryst. Chem.* **1969**, 25, 925–946.
- (24) Wang, L.; Dai, Z.; Zhou, R.; Qu, B.; Zeng, X. C. Understanding the Quenching Nature of Mn⁴⁺ in Wide Band Gap Inorganic Compounds: Design Principles for Mn⁴⁺ Phosphors with Higher Efficiency. *Phys. Chem. Chem. Phys.* **2018**, 20, 16992–16999.
- (25) Adachi, S. Photoluminescence Properties of Mn⁴⁺-Activated Oxide Phosphors for Use in White-LED applications: A Review. *J. Lumin.* **2018**, 202, 263–281.
- (26) Zhang, S.; Hu, Y.; Duan, H.; Fu, Y.; He, M. An Efficient, Broad-Band Red-Emitting Li₂MgTi₃O₈:Mn⁴⁺ Phosphor for Blue-Converted White LEDs. *J. Alloys Compd.* **2017**, *693*, 315–325.
- (27) Chen, T.; Yang, X.; Xia, W.; Li, W.; Xiao, S. Deep-Red Emission of Mn^{4+} and Cr^{3+} in $(Li_{1-x}A_x)_2MgTiO_4$ (A = Na and K) Phosphor: Potential Application as W-LED and Compact Spectrometer. *Ceram. Int.* **2017**, 43, 6949–6954.
- (28) Đorđević, V.; Brik, M. G.; Srivastava, A. M.; Medić, M.; Vulić, P.; Glais, E.; Viana, B.; Dramićanin, M. D. Luminescence of Mn⁴⁺ Ions in CaTiO₃ and MgTiO₃ Perovskites: Relationship of Experimental Spectroscopic Data and Crystal Field Calculations. *Opt. Mater.* **2017**, *74*, 46–51.
- (29) Blasse, G. Influence of Crystal Structure on Luminescence. *Mater. Res. Bull.* **1968**, 3, 807–815.
- (30) Brik, M. G.; Camardello, S. J.; Srivastava, A. M. Influence of Covalency on the $\rm Mn^{4+2}$ $E_{\rm g}$ to $^4A_{2g}$ Emission Energy in Crystals. *ECS J. Solid State Sci. Technol.* **2015**, *4*, R39–R43.
- (31) Brik, M. G.; Srivastava, A. M. Critical Review—A Review of the Electronic Structure and Optical Properties of Ions with d^3 Electron Configuration (V^{2+} , Cr^{3+} , Mn^{4+} , Fe^{5+}) and Main Related Misconceptions. ECS J. Solid State Sci. Technol. 2018, 7, R3079—R3085.
- (32) Zhou, Q.; Dolgov, L.; Srivastava, A. M.; Zhou, L.; Wang, Z.; Shi, J.; Dramićanin, M. D.; Brik, M. G.; Wu, M. Mn²⁺ and Mn⁴⁺ Red Phosphors: Synthesis, Luminescence and Applications in WLEDs. A Review. *J. Mater. Chem. C* **2018**, *6*, 2652–2671.
- (33) Kemeny, G.; Haake, C. H. Activator Center in Magnesium Fluorogermanate Phosphors. *J. Chem. Phys.* **1960**, 33, 783–789.
- (34) Senden, T.; van Dijk-Moes, R. J. A.; Meijerink, A. Quenching of the Red Mn⁴⁺ Luminescence in Mn⁴⁺-Doped Fluoride LED Phosphors. *Light: Sci. Appl.* **2018**, *7*, 8.
- (35) Ruiz, D.; del Rosal, B.; Acebrón, M.; Palencia, C.; Sun, C.; Cabanillas-González, J.; López-Haro, M.; Hungría, A. B.; Jaque, D.; Juarez, B. H. Ag/Ag₂S Nanocrystals for High Sensitivity Near-Infrared Luminescence Nanothermometry. *Adv. Funct. Mater.* **2017**, 27, 1604629
- (36) Kusama, H.; Sovers, O. J.; Yoshioka, T. Line Shift Method for Phosphor Temperature Measurements. *Jpn. J. Appl. Phys.* **1976**, *15*, 2349–2358.
- (37) Zhang, W.; Wang, G.; Cai, Z.; Baxter, G. W.; Collins, S. F. Spectral Analysis for Broadband Fluorescence: Temperature Sensing with the YAG:Ce Phosphor as an Example. *Opt. Mater. Express* **2016**, *6*, 3482–3490.
- (38) Ćirić, A.; Stojadinović, S.; Dramićanin, M. D. Time-Integrated Luminescence Thermometry of Eu³⁺ and Dy³⁺ Doped YVO₄. *Sens. Actuators, A* **2019**, 295, 450–455.